ECS Journal of Solid State Science and Technology, **2** (9) Q131-Q135 (2013)
2162-8769/2013/2(9)/Q131/5/$31.00 © The Electrochemical Society

Effect of Oxygen on the Microstructural Growth and Physical Properties of Transparent Conducting Fluorine-Doped Tin Oxide Thin Films Fabricated by the Spray Pyrolysis Method

N. Chantarat,[a] Yu-Wei Chen,[a] Shu-Han Hsu,[b] Chin-Ching Lin,[c] Mei-Ching Chiang,[c] and San-Yuan Chen[a,z]

[a]*Department of Materials Science and Engineering, National Chiao Tung University, Hsinchu, Taiwan*
[b]*National Nano Device Laboratories, Science-based Industrial Park, Hsinchu, Taiwan*
[c]*Materials and Chemical Research Laboratories, Industrial Technology Research Institute, Chutung, Hsinchu, Taiwan*

We reported the fabrication of an FTO conducting thin film via a spray deposition method, which was used to investigate the effect of oxygen content in the carrier gas on deposited film morphology and properties. Using a carrier gas containing various O_2/N_2 concentrations (0%, 20%, 50%, 80%, and 100%) led to significant changes in the thickness, size, and shape of grain growth. The deposited films with 0–50% oxygen content yielded a low resistivity of $\sim 10^{-4}$ Ω-cm and a transmittance in the range of 76–96% at 550 nm. Furthermore, by changing the carrier gas concentration, the FTO films displayed different charge transport, recombination, and collection properties due to the surface and interfacial effects. These films with modified properties can be applied to dye-sensitized solar cells (DSSCs). Overall, the conversion efficiency of a solar cell based on a 0% O_2 sample was increased by approximately 2% from that of a 100% O_2 sample. The higher efficiency is mainly the result of the lower O_2 content, which minimized the grain boundaries (spacing) and improved the electron transport on the FTO film surface.
 [DOI: 10.1149/2.005309jss]

Manuscript submitted February 12, 2013; revised manuscript received May 14, 2013. Published June 11, 2013.

Transparent conductive oxides (TCOs) have many applications in modern electronics. Because of their high optical transparency and metal-like conductivity, they have been widely used for electrode applications in devices such as thin-film solar cells,[1] optoelectronic devices,[2] gas sensors,[3] frost-resistant surfaces,[4] e-windows,[5] etc. Up to now, most well-known TCO materials such as tin-doped indium oxide (ITO) exhibit n-type conductivity and oxygen deficiency due to oxygen vacancies and possible incorporated oxygen. However, ITO has two obvious disadvantages: (1) Providing a stable supply of ITO for the current expanding market is difficult because of the high price and scarcity of indium. (2) The electrical properties are significantly degraded after an essential annealing process in an oxidizing atmosphere with a temperature over 300°C. Therefore, a substitution for ITO is needed. Fluorine-doped tin oxide (FTO) has been found to be one of most comparable materials to ITO. FTO has attracted much attention as a promising alternative because of its wide energy gap (E_g = 3.67 eV), low cost of production, thermal stability, chemical inertness, and high transparency, although lower conductivities compared with the $\sim 10^{-4}$ S/cm of ITO hinder its commercial applications. In addition, FTO thin films have been extensively prepared by various methods, such as chemical vapor deposition (CVD), metallorganic deposition, rf sputtering, sol–gel, and spray pyrolysis deposition (SPD).[6–8]

Considerable effort has gone into investigating how to develop a textured surface on FTO conducting electrodes to improve the performance of solar cell devices by reducing light reflection or making light scattering more efficient. An anisotropic post-etching method using lithographic patterning and etching steps is typically used to achieve the desired morphology.[9,10] However, this might be deleterious to the film properties and difficult to control and could increase processing costs. Therefore, this becomes an important issue for developing high surface roughness and quality stable films during growth. For example, fabricating self-textured films via several methods, the electrical resistivity of PLD-grown 210–1000 nm thick FTO films was reported to be in the range of 2-3 mΩ-cm,[11] and an MOCVD-grown FTO film with a similar thickness possessed a resistivity value in the range of 1.2-2.1 Ω-cm.[12]

Among the various techniques, spray pyrolysis deposition (SPD) has been economically conducted to produce self-textured FTO films with a simple scalable deposition and easy doping process that depends on manipulation of the substrate temperature, calcinations, gas pressure, and flow rate. On the basis of the proposed principle, the variation in the growth and nucleation of deposited FTO films is strongly determined by the incorporated oxygen concentration, which has an effect on the surface mobility and the oxidation rate of chemical precursors.

In the present work, we report the effect of the oxygen content in the carrier gas on the FTO film morphology and optoelectronic properties during the spray pyrolysis deposition. The deposition of 400–550 nm thick films on a glass substrate led to significant changes in the thickness, size, and shape of grain growth, which is indicative of variable correlation between optical and electrical properties. Here, our deposited films reach a low resistivity of $\sim 10^{-4}$ Ω-cm and a transmittance of 76%∼96% at 550 nm. Finally, the photovoltaic implementation of dye-sensitized solar cells (DSSCs) and electrochemical impedance spectroscopy (EIS) also revealed particular behaviors, such as the charge transport, recombination, and collection properties of the surface and interfacial effects. Consequently, the higher growth rate for spray pyrolysis deposition compared with other methods provides an improved understanding of the grain growth mechanisms of FTO film because various surface morphologies could be obtained by using high deposition temperatures in air. Moreover, other parameters, including deposited temperature, duration, gas flow rate, and spray gun settings, could be further optimized to produce better electrical and optical film properties, leading to a significant enhancement of efficient solar cell devices.

Experimental

Fluorine-doped tin oxide films (SnO_2:F) were deposited over Corning glass substrates by ultrasonic spray pyrolysis. The precursor solution containing a mixture of $SnCl \cdot 4H_2O$ (1 mM) and NH_4F (0.5 mM) was dissolved in 500 mL of DI water. To improve the solubility of the solution, 10 mL of HCl was added to the solution and stirred vigorously (∼30 min) until the solution turned transparent. The product solution was placed in an ultrasonic nebulizer reactor, which can produce an aerosol with a controlled droplet size. The experimental apparatuses consist of a specific homemade ultrasonic atomizer, spray gun, and graphite hotplate. The deposition parameters, such as substrate temperature, spray rate, and distance from the spray gun to the substrate, were kept constant at the optimized value: 400°C, 20 mL/min, and 30 cm, respectively. In addition, different morphologies of textured FTO films can be obtained by applying a carrier gas containing O_2 and N_2 during the deposition process (O_2: 0%, 20%, 50%, 80%, and 100%).

[z]E-mail: sanyuanchen@mail.nctu.edu.tw

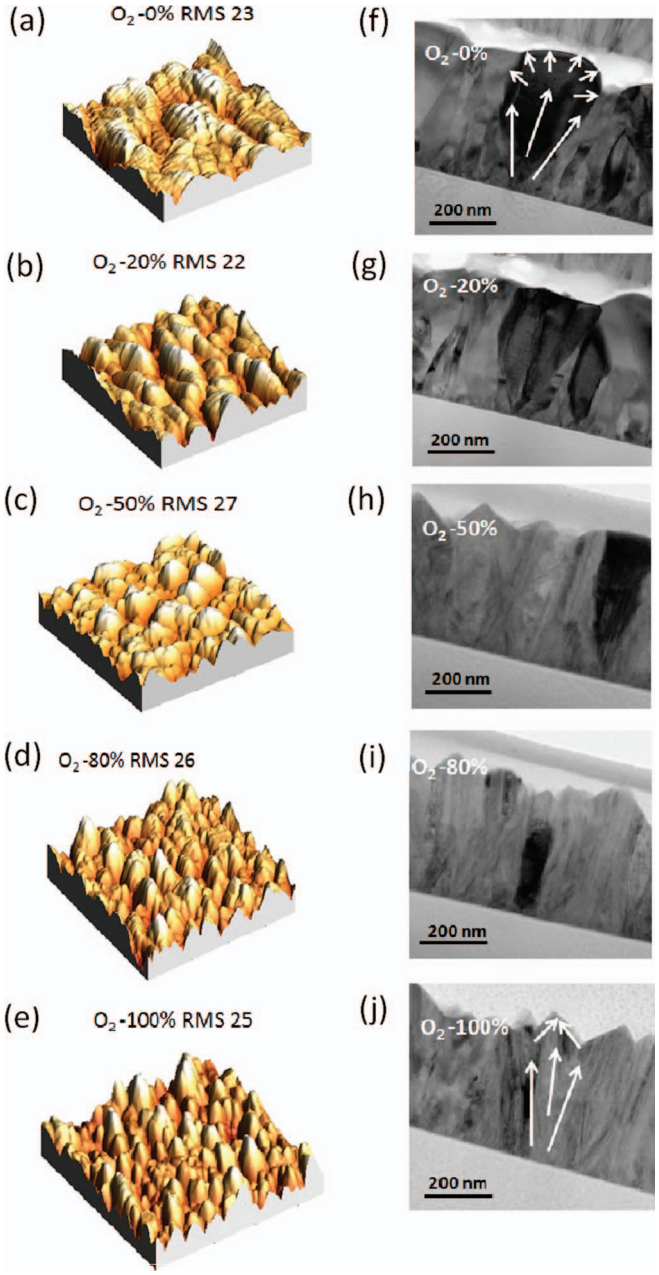

Figure 1. (a–e) AFM topographic 5 × 5 μm scans and (f–j) cross-sectional TEM images for oxygen-incorporated FTO films deposited at various oxygen concentrations: 0%, 20%, 50%, 80%, and 100%.

A morphology analysis (i.e., roughness, grain size, and other cross-sectional observations) of the samples was performed by a field-emission scanning electron microscope (SEM, JEOL JSM-6700F), a high-resolution transmission electron microscope (TEM, JEOL 2100) operated at 200 keV, and an atomic force microscope (AFM). The crystal structures were determined using an XRD diffractometer equipped with a Cu Kα radiation source ($\lambda = 0.154$ nm), and the diffraction data were collected for $2\theta = 10\sim70^\circ$. For the optical analysis, a UV-VIS double beam spectrophotometer (Model: Evolution 300 BB) was employed to record the optical transmission spectra of the deposited films over the wavelength range of 300–700 nm. Hall effect measurements were carried out at room temperature with a van der Pauw sample configuration (magnetic field: 4000 Gauss, electric current: 0.1 mA), using indium balls as the ohmic electrode, to demonstrate electrical properties such as carrier concentration (n), resistivity (ρ), and mobility (μ). For device performance, dye-sensitized solar cells (DSSCs) were fabricated using N3 dye, TiO_2 sol, liquid electrolyte, and a Pt counter electrode. The photovoltaic properties, including short-circuit current density (J_{sc}), open-circuit voltage (V_{oc}), and conversion efficiency (η), were measured under AM 1.5 sunlight illumination (Model YSS-80, Yamashita Denso, Japan; intensity: 100 mW/cm^2) from an illuminated area of 0.5 cm × 0.5 cm. The electrochemical impedances of the cells were also measured using the photocurrent-potential-impedance analyzer by applying an open-circuit voltage as the bias in the frequency range of 0.1 Hz - 1 MHz.

Results and Discussion

Based on our spray pyrolysis method, different O_2/N_2 concentrations (0%-100%) serve as the carrier gas for depositing the FTO films with different surface morphologies. The grain size, estimated from the top AFM images (Figure 1a–1e), is apparently smaller for films with a higher O_2 content. The optimized deposition temperature (constant at 400°C) and duration (varied by 5–10 min) were used for all film types to form films with a similar thickness in the range of 400–450 nm, as indicated in the cross-sectional TEM images (Figure 1f–1j). As a result, the surface roughness (RMS) varies in a small range of 22–27, and the thickness was slightly increased. This behavior was more pronounced for higher O_2 concentrations. Two types of growth for FTO films can be classified in two cases: island-like structures at low O_2 content (0%-20%) and pyramid-like structures at high O_2 content (50%-100%). The side-view TEM images reveal the grain growth mechanism, as indicated in the figures. The first type of film may exhibit strong lateral grain development rather than grain boundary scattering; therefore, dense and thick films were grown in geometrical directions with circular coverage. In contrast, in the second type of film, it is possible that a higher oxygen concentration will suppress the lateral growth and individually form cone seeds with apexes. The nucleation site density becomes much higher than that of the first type due to the effect of the low surface energy at higher oxygen concentrations. Moreover, the low-magnification SEM images in Figure 2a–2c illustrate the top views of a portion of the large-area FTO films (O_2: 0%, 20%, and 100%, respectively). An examination of the surface morphology shows how the high-density microstructural

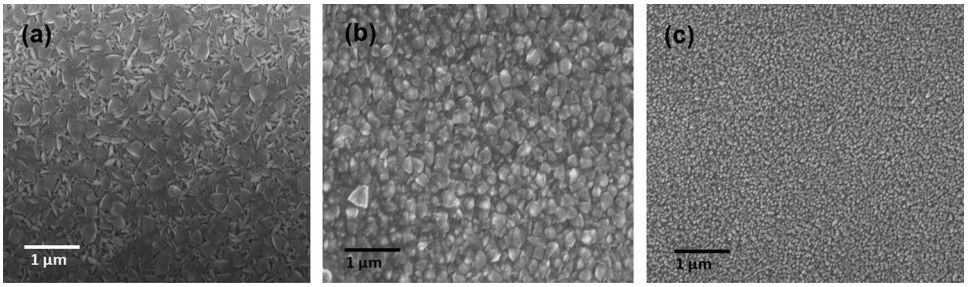

Figure 2. FE-SEM images of the deposited FTO films on Corning glass as a function of oxygen content: (a) 0%, (b) 20%, and (c) 100%.

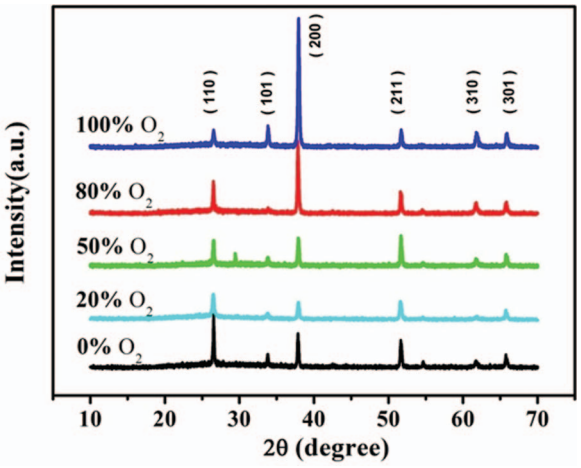

Figure 3. X-ray diffraction (XRD) patterns of FTO films deposited on glass substrates with various concentrations of incorporated O.

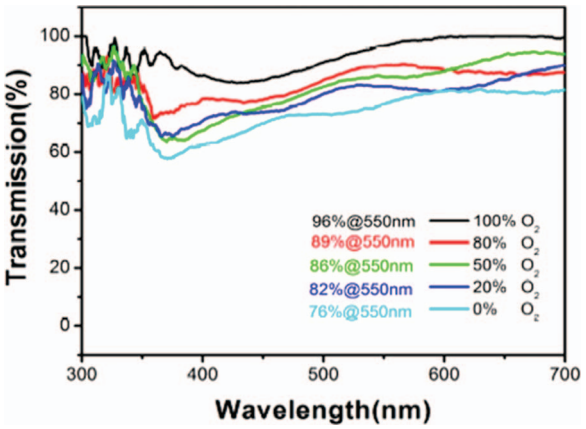

Figure 4. Transmission (T%) spectra of FTO films with varying oxygen concentrations, deposited on Corning glass.

grains are homogeneously fabricated in an array over a large area with a certain size. The films are very compact, but the textural boundaries are clearly visible, and the result shows a correlation with the AFM and TEM images.

According to nucleation theory, the nucleation density (N) can be expressed by the following equation:

$$N = A\exp\left(\frac{-\Delta G}{RT}\right)$$

where ΔG is the activation energy of nucleation, which is composed of the volume free energy (ΔG_V) and the surface free energy (ΔG_S). R, T, and A are the gas constant, growth temperature, and a constant, respectively. Earlier research explained that the change in the volume free energy decreases as the content of O_2 in the ambient atmosphere of the deposition process increases. Thus, the activation energy of nucleation becomes lower under O-rich conditions, which enhances the surface mobility for the formation of the initial layer of the FTO film, resulting in smaller grains.[13]

The XRD pattern in Figure 3 reveals the evolution of FTO thin films with varied contents of O_2/N_2 carrier gas. All the FTO films are polycrystalline, indicating a SnO_2 rutile (tetragonal) structure without additional peaks for SnO or Sn phases. As-deposited FTO film (O_2: 0%) shows the preferential orientation of (110), (200), and (211) at 26.5, 38, and 51.5 degrees, respectively. When the oxygen content was increased, i.e., 80% and 100%, the (200) peak monotonically dominated the patterns, and the (110) peak decreased. The intensity ratio between (110) and (200) decreases from 1.3 to 0.7, corresponding to a change in the carrier gas from pure nitrogen (O_2: 0%) to pure oxygen (O_2: 100%). In principle, this particular orientation can be influenced by the grain evolutionary selection that follows the concept of periodic bond chain theory:[1,4] the thermodynamic equilibrium form of the SnO_2 structure typically shows a dominant (110) plane of polar faces composed of both tin and oxygen atoms. However, Korotkov et al. reported that the addition of a high concentration of oxygen may enhance the presence of the polar halogen-rich region due to the formation of by-product HCl from the spray pyrolysis process,[5] leading to quenching of the [110] growth direction and growth rate saturation. In contrast, for a low surface energy at a high oxygen concentration, it was found that (200) deposition could be induced by the formation of a seed layer, which allowed the enhanced nucleation density to change the orientation of the above layer, forming a highly texture surface useful for TCO applications.

In Figure 4, the overall transmission of the films was characterized by UV-Vis measurements. The 100% O_2 sample shows the highest percentage in transmission (96% at the wavelength of 550 nm). Furthermore, the samples with the lower O_2 content of 0%, 20%, 50%, and 80% have lower transmission values at 76%, 82%, 86%, and 89%, respectively. The evaluation results can be explained by a correlation of light scattering and reflection, depending on the size and shape of the grain structures. As shown above, the first result is attributed to an enhanced scattering at the surface and the internal layer and diffraction at structures with sizes close to the wavelength of a photon (Figure 1). This behavior is due to the smaller grain growth with a high density in a definite area compared with what occurs for lower O_2 concentrations. Note that the theoretical consideration of this behavior also refers to an increase in waveguide sensitivity. At 80% and 100%, the fluctuation of frequent waves can be clearly observed due to a high surface texture, e.g., the pyramid-like nanostructure together with a large refractive index (n). In contrast, a dome-like structure with a flat grain surface may give rise to the possibility of light reflection, which results in the loss of the surface-normal incidence based on the Fresnel effect.[14,15] The desired sideways waveguiding behavior is somewhat reduced because the dome with a large incident angle acts as an individual converging lens, only redirecting the light in the forward and backward direction, with less internal diffusion.

Figure 5 shows the electrical properties of FTO film at room temperature as a function of the oxygen content of the carrier gas (0%, 20%, 50%, 80%, and 100%), including the carrier concentration (n), resistivity (ρ), and Hall mobility (μ). The carrier concentration increased to 16.12×10^{20} cm^3 at 50% and then leveled off for further increases in the oxygen content. In a consistent manner, the values of resistivity increased to 18 Ω-cm and 70 Ω-cm at 80% and 100%, respectively. As indicated by the above results, increasing the oxygen

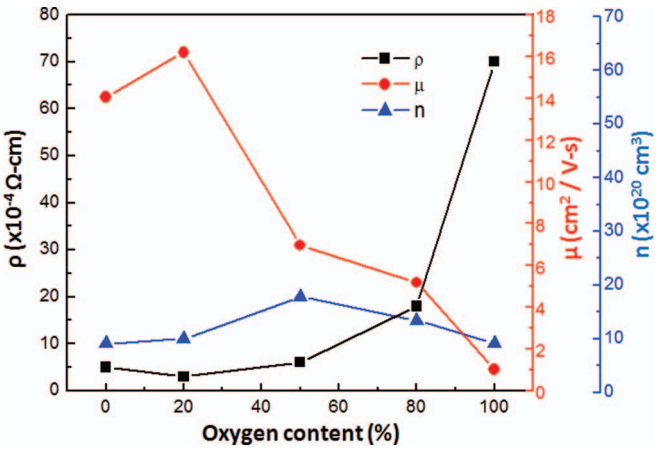

Figure 5. FTO film electronic transport properties: carrier concentration (n), resistivity (ρ), and Hall mobility (μ) as a function of the oxygen concentration (0-100%).

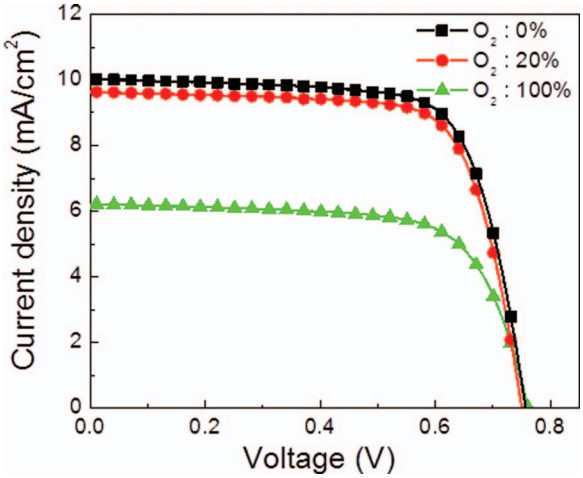

Figure 6. J-V characteristics of FTO film-based DSSCs. The illumination intensity of 100 mW cm^{-2} with AM 1.5 and an active area of 0.25 cm^2 were applied.

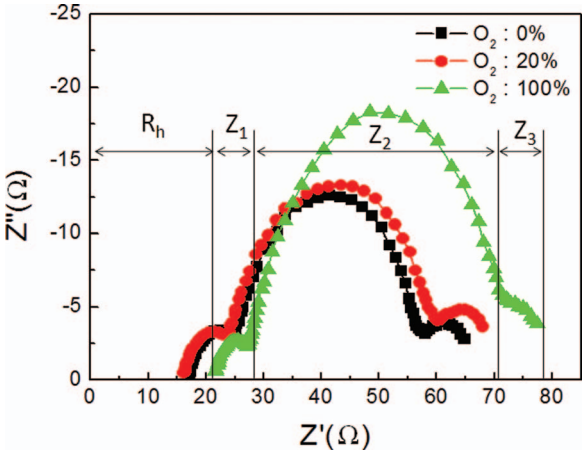

Figure 7. Representative Nyquist plot of the electrical impedance spectra of the FTO films measured in the frequency range of 0.1 Hz – 1 MHz under AM 1.5.

content up to 50% is expected to improve the internal oxidization of metallic Sn, which forms well-dispersed SnO_2. Instead, at oxygen concentrations above 50%, the excessive oxygen ions (O^{2-}) generated from O_2 molecules at high working temperatures (> 300°C) might predominantly disrupt the stoichiometric FTO film by reducing the amount of intrinsic donor defects (and Sn_i^{4+}). Thus, the O^{2-} ion will serve as a compensating acceptor defect to trap free electrons and raise the height of the potential barrier along grain boundaries, resulting in a lower carrier concentration and a higher resistivity in the matrix. Additionally, the mobilities were as high as 14.45 cm^2/V-s at 0% and 16.25 cm^2/V-s at 20% because the formation of large grains allows a smoother surface to develop compared with other films with higher oxygen contents. Thus, the mobility significantly decreased to 1.17 cm^2/V-s at 100% because the small grain size and numerous boundaries between the grains hindered the intergrain carrier mobility. Due to the increased grain boundary and ionized impurity scattering of the carriers, the electrical properties tend to degrade in proportion to the oxygen concentration.

The photovoltaic properties of the textured FTO film-based DSSCs with different amounts of incorporated O_2 (0%, 20%, and 100%) in the films are summarized in Figure 6 and Table I. At 100%, the conversion efficiency (η) obtained is as low as 3.22%; it then increased to 4.98% and 5.25% at O_2:20% and O_2:0%, respectively. This is mainly due to the increased short-circuit current density (J_{sc}) from 6.20 to 9.65 and 10.03 mA/cm^2, respectively, although the open-circuit voltage (V_{oc}) was not changed much (it only varied in the range of 0.750–0.761 V). Because V_{oc} strongly depends on recombination or back-electron transport, the high values with only a small variation could be associated with suppressing those effects, resulting in high electron throughput. In contrast, a large change in J_{sc} is indicated by differences in grain boundaries (spacings) in each case, which can affect electron transport on the FTO film surface (as described by Hall measurements) and the interfacial pathway (contact area) between the TiO_2 layer and the FTO film. Moreover, due to abundant O_2 incorporation, the low electrical characteristics (ρ and μ) of the 100% O_2 sample were assumed to dominate the performance of DSSCs, although the film showed the highest transmission in the UV-Vis analysis (Figure 4).

Table I. Summary of FTO film properties used in DSSCs.

O_2-content	V_{oc} (V)	J_{sc} (mA/cm^2)	FF (%)	H (%)
0%	0.756	10.03	0.692	5.25
20%	0.750	9.65	0.688	4.98
100%	0.761	6.20	0.682	3.22

Due to the grain boundary effect mentioned above, we further examined the correlation between the cell performance and the internal resistance of the DSSCs via electrochemical impedance spectroscopy (EIS) measured at V_{oc} under 1.5 AM (Figure 7). Regarding the significant difference in surface morphology (grain growth), the 0%, 20%, and 100% O_2 samples were used to elucidate the behavior of the electron interception and the electron diffusion to the collecting anode. The Nyquist plots of the samples exhibited four impedance components of a DSSC, including the resistance element (R_h) of the FTO layer in the high-frequency region (> 10^6 Hz) and the other three impedance elements Z_1 (ω_1: 10^3-10^5 Hz), Z_2 (ω_2: 1-10^3 Hz), and Z_3 (ω_2: 0.1-1 Hz) associated with charge transfer processes at the counter electrode, the interfaces between the FTO/TiO_2/dye/electrolyte, and the Nernstian diffusion within the electrolyte, respectively. A specific feature of the Z_2 curve for the 100% O_2 sample increased by 11.5 Ω in width compared with those of the 0% and 20% samples, which is attributed to the electrochemical interfacial resistance between the FTO and the TiO_2 working electrode. Simultaneously, the R_h of the 100% O_2 sample also increases by 6 Ω, showing good agreement with the electrical properties of the Hall measurement in Figure 4, whereas the other values (Z_1 and Z_3) remain almost identical.

Conclusions

In summary, fluorine-doped tin oxide (FTO) electrodes have been investigated as an alternative anode to indium tin oxide (ITO) in dye-sensitized solar cells (DSSCs). FTO films were grown by ultrasonic spray pyrolysis deposition on Corning glass substrates at 400°C using O_2/N_2 deposition concentrations of 0, 20, 50, 80, and 100%. The structural, electrical, and optical properties of the FTO texture films were studied as a function of surface morphology. A significant reduction in grain size was found to increase the surface roughness, which depended strongly on the increased oxygen concentration. In contrast, the formation of a flattened film is a crucial point that reduces the film resistivity (ρ) to 10^{-14} Ω-cm and enhances the transmittance (T%) up to 96% at 550 nm. Moreover, electrochemical impedance spectroscopy (EIS) indicates that a flat surface can minimize the discontinuity of TiO_2 particles on an FTO textured film. The key improvements in the electrical and optical properties reduced the Auger recombination, so the photovoltaic performance of FTO film-based DSSCs with 0% O_2 showed a higher conversion efficiency (5.25%) compared with DSSCs with 100% O_2 (3.22%); the numerous grain boundaries and pyramid-shaped structures made a significant contribution to the degradation of the electron transport (diffusion length).

Acknowledgments

This work was financially supported by the National Science Council of the Republic of China, Taiwan, under Contract NSC100-3113-E-009-002. We also thank the Industrial Technology Research Institute of Taiwan for technical and financial support.

References

1. I. Volintiru, M. Creatore, B. J. Kniknie, C. I. M. A. Spee, and M. C. M. Van De Sanden, *Journal of Applied Physics*, **102**, 043709 (2007).
2. S. Lee, J. H. Noh, H. S. Han, D. K. Yim, D. H. Kim, J.-K. Lee, J. Y. Kim, H. S. Jung, and K. S. Hong, *The Journal of Physical Chemistry C*, **113**, 6878 (2009).
3. J. H. Lee, C. Y. Chou, Z. X. Bi, C. F. Tsai, and H. Wang, *Nanotechnology*, **20**, 395704 (2009).
4. C. Y. Kim and D. H. Riu, *Thin Solid Films*, **519**, 3081 (2011).
5. R. Y. Korotkov, P. Ricou, and A. J. E. Farran, *Thin Solid Films*, **502**, 79 (2006).
6. J. Kane and H. P. Schweizer, *Journal of the Electrochemical Society*, **123**, 270 (1976).
7. T. N. Blanton and M. Lelental, *Materials Research Bulletin*, **29**, 537 (1994).
8. K. Y. Rajpure, M. N. Kusumade, M. N. Neumann-Spallart, and C. H. Bhosale, *Materials Chemistry and Physics*, **64**, 184 (2000).
9. C. Xiang, S.-C. Kung, D. K. Taggart, F. Yang, M. A. Thompson, A. G. Güell, Y. Yang, and R. M. Penner, *ACS Nano*, **2**, 1939 (2008).
10. D.-G. Choi, H. K. Yu, S. G. Jang, and S.-M. Yang, *Journal of the American Chemical Society*, **126**, 7019 (2004).
11. H. Kim, G. Kushto, R. Auyeung, and A. Piqué, *Applied Physics A: Materials Science & Processing*, **93**, 521 (2008).
12. J. W. Bae, S. W. Lee, and G. Y. Yeom, *Journal of the Electrochemical Society*, **154**, D34 (2007).
13. K. Omura, P. Veluchamy, M. Tsuji, T. Nishio, and M. Murozono, *Journal of the Electrochemical Society*, **146**, 2113 (1999).
14. M. Dashtdar and M. T. Tavassoly, *J. Opt. Soc. Am. A*, **25**, 2509 (2008).
15. H. Fouckhardt, I. Steingoetter, M. Brinkmann, M. Hagemann, H. Zarschizky, and L. Zschiedrich, *Advances in OptoElectronics*, **2007**, 1 (2007).